Potential of an Al-Ti-$MgAl_2O_4$ Master Alloy and Ultrasonic Cavitation in the Grain Refinement of a Cast Aluminum Alloy

V.M. SREEKUMAR, N.H. BABU, and D.G. ESKIN

A new grain refining master alloy containing $MgAl_2O_4$ and Ti was synthesized by *in situ* reaction of TiO_2 particles in an Al-Mg melt. $MgAl_2O_4$ particles formed were distributed in the melt by ultrasonic cavitation processing. The obtained master alloy showed considerable (50 pct) grain refining ability in a commercial A357-type Al-Si alloy. Ultrasonication contributed further to 25 pct in the grain refinement. In comparison with a commercial Al-5 pct Ti-1 pct B master alloy, the efficiency of the new master alloy is less at a lower addition rate. Nevertheless, both master alloys performed similarly at higher additions. The strength and ductility of the inoculated and ultrasonicated alloy showed at least a 10 pct and a 50 pct increase, respectively, as compared with non-grain-refined alloy and a similar mechanical performance in comparison with the alloy inoculated with Al-5 pct Ti-1 pct B master alloy.

DOI: 10.1007/s11663-016-0824-5

I. INTRODUCTION

GRAIN size is one of the most important factors that influences the processing and properties of Al alloys, and grain refinement is considered to be the foremost technique for achieving improvement in the quality of cast products, eliminating coarse and columnar grains, minimizing casting defects such as hot tear or macrosegregation, and facilitating downstream processing of the cast products.[1–5] From the various grain refinement techniques, the most common practice is the addition of specialized master alloys containing potent nucleation substrates (TiB_2, TiC, AlB_2), primary intermetallics (Al_3Ti, Al_3Nb, *etc.*), and/or growth-restricting alloying elements (Ti, V, Nb, *etc.*).[6–10] In current industrial practice, Al-Ti-B (Al-Ti-TiB_2) and Al-Ti-C (Al-Ti-TiC) master alloys are the most common grain refiners used in cast and wrought Al alloys.[2,3] The grain refinement mechanisms as well as some technological issues related to Si or Zr poisoning of Al-Ti-B grain refiners are thoroughly scrutinized by theoretical models and experiments.[11,12] Despite the commercial success of Al-Ti-B and Al-Ti-C grain refiners, some drawbacks are related to their application such as reduced performance in high-Si- or Zr-containing alloys and agglomeration of borides in Al-Ti-B master alloys and a narrow process-parameter window for Al-Ti-C master alloys.[1,2,5,6,12] A search for new grain refining systems that may substitute that currently used is ongoing. In recent times, interest has grown on using oxides such as Al_2O_3, $MgAl_2O_4$, and MgO as nucleation substrates in Al.[13–15] It is well known that these oxides are formed naturally on the aluminum melt surface as stable layers, being thermodynamically stable and having sufficiently good crystallographic match with solid aluminum to act as substrates for its nucleation.[13] Similarly, these oxides can be formed *in situ* as a reaction product of externally added oxide particles and liquid aluminum.[16] In the case of thermodynamically unstable oxides (*e.g.*, volatile oxides such as SiO_2) added externally in liquid aluminum, formation of stable oxide crystals can be maximized by complete conversion of the volatile oxides.[17] The same reactions were demonstrated upon conversion of volatile oxides into interconnected fibers of $MgAl_2O_4$ (spinel) phase in an Al alloy by self-propagating, high-temperature synthesis of powder compacts.[18,19]

It was reported that oxide particles work better as nucleating substrates when the melt is subjected to an external physical field. Atamanenko *et al.*[20] reported improved nucleation of aluminum on synthetic Al_2O_3 particles after ultrasonic cavitation melt processing. Li *et al.*[13] demonstrated grain refinement of Al-Mg alloys using an intensive melt shearing technique and proposed a mechanism related to the dispersion of naturally occurring oxides such as $MgAl_2O_4$ in Al alloys. More recently, a significant reduction in grain size was observed in Al-$MgAl_2O_4$ *in situ* composite, presumably caused by $MgAl_2O_4$ crystals dispersed in aluminum by ultrasonic melt treatment.[21]

This article reports on the manufacturing of an Al-$MgAl_2O_4$ concentrated master alloy and its application as a grain refiner in a commercially important cast alloy. First, the synthesis of the oxide-based grain

V.M. SREEKUMAR, Research Fellow, and N. HARI BABU, Reader, are with the Brunel Centre for Advanced Solidification Technology (BCAST), Brunel University London, Waterside House, Cowley Business Park, Uxbridge UB8 2HP, United Kingdom. Contact e-mail: vm.srees@gmail.com, Sreekumar.VadakkeMadam@brunel.ac.uk D.G. ESKIN, Professor, is with the Brunel University London, and with Tomsk State University, 634050, Russia.

Manuscript submitted July 5, 2016.
Article published online October 24, 2016.

refiner master alloy containing *in situ* $MgAl_2O_4$ particles is described as based on the TiO_2 reaction with an Al-Mg melt assisted by ultrasonication. The reason for the selection of TiO_2 is twofold: (1) The new oxide-based master alloy (Al-Ti-$MgAl_2O_4$) contains free Ti as an important growth restriction element and $MgAl_2O_4$ as a nucleation substrate. (2) The grain refiner species are naturally formed by thermodynamically feasible reactions between Al-Mg melt and TiO_2 at practically acceptable processing temperatures. The possible mechanisms of the formation and dispersion of *in situ* $MgAl_2O_4$ and Ti in Al are discussed and the grain refinement potential of the $MgAl_2O_4$ containing master alloy and its influence on the mechanical properties are examined for an A357-type casting aluminum alloy.

II. EXPERIMENTAL PROCEDURE

Commercially pure (CP) Al (0.08 wt pct Si, 0.1 wt pct Fe, remaining Al) and CP Mg (99.97 wt pct) were taken as initial metals. TiO_2 (Rutile) was chosen as a solid oxygen source for $MgAl_2O_4$ formation. TiO_2 is not stable in liquid aluminum and readily reacts with it to form Al-based oxides.[22] The particle size of the TiO_2 supplied by Sigma-Aldrich was varied from 0.5 to 10 μm (more than 80 pct between 1 and 5 μm). A total of 2 wt pct of TiO_2 particles was stirred in a molten Al-1.5 wt pct Mg alloy at temperatures between 923 K and 973 K (650 °C and 700 °C) using a mechanical impeller made from a Ti alloy and coated with a high-temperature ceramic material to minimize impeller erosion during processing. The total volume of the processed melt was 1 kg. After stirring and mixing, the melt was heated and held at 1173 K (900 °C) for 30 minutes to facilitate the reaction between oxide particles and liquid Al–Mg alloy. Then temperature was decreased to 973 K to 993 K (700 °C to 720 °C), and the melt was subjected to ultrasonic processing (water-cooled Reltec transducer, 17.5-kHz, 3.5-kW, 40-μm peak-to-peak amplitude, Nb sonotrode) while stirring with the impeller for 5 minutes to ensure the dispersion of formed $MgAl_2O_4$ particles and to complete the reaction of TiO_2 particles. The cycles of higher temperature holding and lower temperature mixing were repeated five times, and the final mixture was cast at 1023 K (750 °C) in a steel round mold preheated at 473 K (200 °C). The obtained cast sample would be used as a master alloy (MA), and its average chemical composition was estimated as follows. To measure the chemical composition, 10 g of the master alloy was diluted in 100 g of CP Al and cast in a metallic mold. The average Ti and Mg composition of the cast sample was determined from five measurements on the sample surface by optical emission spectrometry in Foundry Master. The $MgAl_2O_4$ content in the master alloy was calculated using the following reaction:

$$[Mg] + 2[Al] + 2<TiO_2> = <MgAl_2O_4> + 2[Ti] \quad [1]$$

The accuracy of chemical analysis was within 10 rel pct of the average measured value.

Grain refinement efficiency was assessed using an A357-type alloy (7.4 wt pct Si, 0.5 wt pct Mg, 0.1 wt pct Fe, 0.1 wt pct Ti, remaining Al) (500-g level). Different amounts of the master alloy (specified later in the text) were added to 500 g of the molten A357 alloy at 1033 K (760 °C), and the melt was allowed to rest for 5 minutes. After that, the alloy was cast at 1023 K (750 °C) in a steel mold (200 g, cooling rate ~2 to 3 K/s (2 to 3 °C/s)) preheated to 523 K (250 °C). The dimensions of the mold as well as the section where the metallographic samples were taken are shown in Figure 1. In addition to the described experiments, the A357 alloy with and without additions was treated with ultrasound for 3 minutes at 1013 K to 1023 K (740 °C to 750 °C) prior to casting (ultrasonic processing parameters were the same as shown earlier for the master alloy). For comparison, the grain refinement of the A357 alloy was studied after additions of an Al-5 pct Ti-1 pct B master alloy (London Scandinavian Metallurgical Co. Ltd) with all other conditions retained. At least two castings were produced for each condition. The cast samples were ground using SiC paper (400 to 2500 grid size) and polished using OPS. For identification of grain size, polished samples were anodized using 4 pct HBF_4 solution for ~1 minutes at 20 VDC and analyzed in polarized light in an optical microscope (Zeiss Axioscope). The microstructure of the master alloy was investigated using optical microscopy (OM) (Zeiss Axioscope) and scanning electron microscopy (SEM) (Zeiss Supra 35VP), and phase identification was performed using X-ray diffraction (XRD) (Bruker D8 Advance) and energy-dispersive spectroscopy (EDS) (EDAX).

Grain size was determined using the conventional linear intercept method with 50 to 100 grains measured in each sample and with the statistical analysis of the data performed (error bars are shown in relevant plots). The size of the particles was also measured using the linear intercept method with 20 to 50 particles measured and with the statistical error not exceeding 10 rel pct of the average.

Thermal analysis during solidification of selected samples with and without addition of the master alloy was performed using K-type 0.5-mm thick thermocouples and NI-LABVIEW Data Logger capable of collecting 100 data points per second. The accuracy of the temperature measurement was within 0.5 K (0.5 °C). The same steel mold used for grain refinement study was covered with ceramic wool to minimize the temperature loss and preheated to 623 K (350 °C). The thermocouple was positioned from the top between the center and the wall of the mold. The metal was poured at a superheat of 100 K (100 °C) above the liquidus of the alloy. Each experiment was repeated three times with good reproducibility of the results.

Tensile tests of machined specimens (four samples for each condition) were carried out in Instron 5569 with a 50-kN load cell (ASTM E8). The sample dimensions were according to ASTM standard B557-06. Rectangular specimens with gauge length 25 mm were machined from the billet cast in a permanent steel mold (1-kg melt charge). The casting conditions (temperature, melt

treatment) were kept similar to those described earlier. Prior to testing, all test bars were heat treated. The samples were annealed for 12 hours at 813 K (540 °C), water quenched [warm at 323 K (50 °C)], and subsequently aged at 443 K (170 °C) for 12 hours. Elongation of the samples was recorded using an external extensometer (25-mm gauge length), and yield stress was calculated by the 0.2 pct offset method. At least four samples were tested for each condition, and statistical analysis of the data was performed.

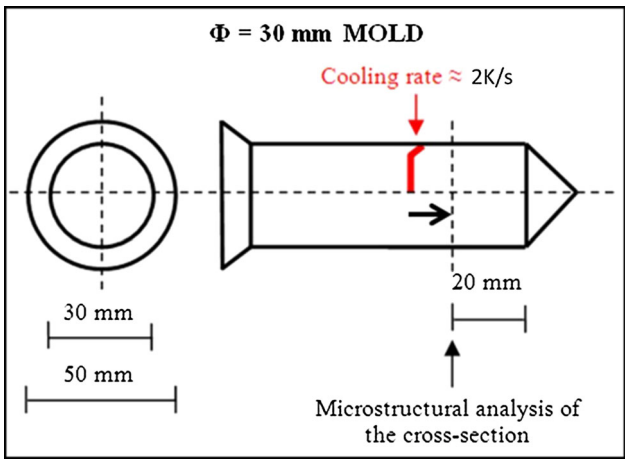

Fig. 1—Schematic of metallic mold used for grain refinement studies.

III. RESULTS AND DISCUSSION

A. *Synthesis of an Al-Ti-$MgAl_2O_4$ Master Alloy*

1. *Chemical and phase composition of the synthesized master alloy*

The average chemical composition of the master alloy was estimated from the chemical analysis as Al-0.6 wt pct Mg-1.3 wt pct Ti-1.8 wt pct $MgAl_2O_4$. We can see that 1.3 wt pct of free elemental titanium was released after the reaction between 2 wt pct TiO_2 and Al according to Eq. [1]. The range of Ti detected in various samples was between 1.2 and 1.5 wt pct probably as a result of a minor Ti dissolution from the impeller. Also, 0.6 wt pct Mg was found to remain in the alloy after the reaction and oxidation (burning) at higher temperatures. Figure 2 shows the microstructures of the Al-Ti-$MgAl_2O_4$ master alloy prepared by the *in situ* synthesis. $MgAl_2O_4$ particles (dark spots) were found dispersed mostly as small clusters in the Al matrix (Figures 2(a) and (b)). Clusters of 10 to 20 μm were also identified everywhere in the cast billet, although large ones (>50 μm) were rarely observed. Al_3Ti blocks and platelets (pointed by arrows) were found distributed in the matrix alloy (Figures 2(a) and (b)). Al_3Ti particles were also identified within the clusters of $MgAl_2O_4$ as illustrated in Figure 2(c). In general, the microstructure of the master alloy is comparable with that of a commercial Al-5Ti-1B master alloy where Al_3Ti blocky particles of size ~50 μm and fine TiB_2 particles were distributed throughout the matrix (Figure 2(d)). The presence of $MgAl_2O_4$ and Al_3Ti phases is confirmed in Figures 3 , 4, and 5. An XRD pattern of the cast billet showed only $MgAl_2O_4$ and Al_3Ti peaks in the master alloy (Figure 3). No unreacted TiO_2 particles were

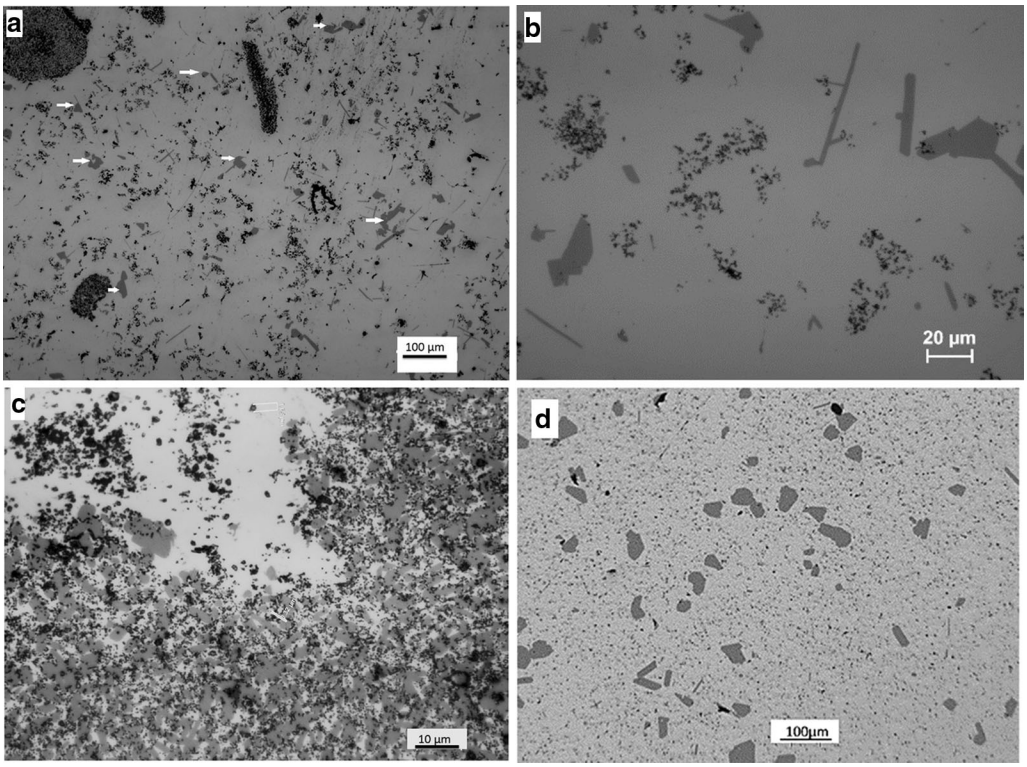

Fig. 2—Optical micrographs of (*a* through *c*) Al-Ti-$MgAl_2O_4$ master alloy and (*d*) Al-5Ti-1B master alloy.

identified. The formation of $MgAl_2O_4$ and Al_3Ti in the master alloy was confirmed also by SEM coupled EDS analysis (Figures 4 and 5). The size of $MgAl_2O_4$ particles varied from a few hundred nm to 1 to 2 μm. Similarly, most Al_3Ti particles were found to be between 1 and 20 μm in size.

2. *Formation of $MgAl_2O_4$ in the master alloy*

The Al_2O_3-$MgAl_2O_4$-MgO phase equilibria was studied by thermodynamic models and experimentally verified with different Mg compositions of matrix alloy elsewhere.[23] The studies established that Al_2O_3 forms at very low Mg content (<0.19 wt pct), whereas $MgAl_2O_4$ is stable between 0.007 and 10 wt pct Mg and MgO is stable at >7 wt pct Mg. Hence, in the Al-1.5 wt pct Mg-2 wt pct TiO_2 composition used in the present study, only $MgAl_2O_4$ can be stable, which was confirmed by XRD analysis (see Figure 3). The synthesis of spinel is initiated by reactive wetting through Eq. [1] as it results in the reduction in interfacial energy (ΔG° = –273 KJ/mol at 1123 K (850 °C)) by the formation of $MgAl_2O_4$ at the liquid Al-TiO_2 interface (event (a) in Figure 6).[24] The released Ti reacts with Al to form Al_3Ti.

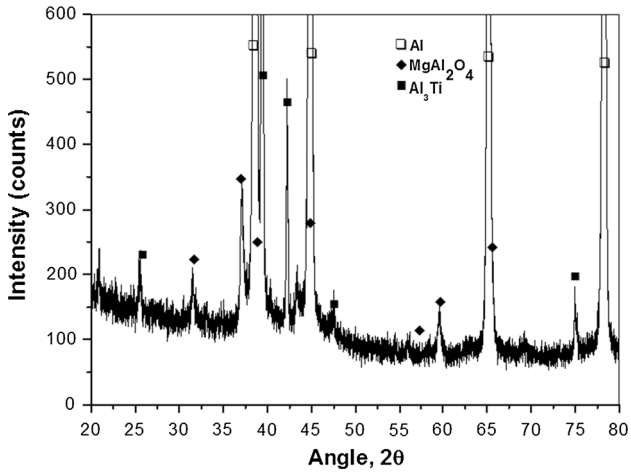

Fig. 3—X-ray diffraction of Al-Ti-$MgAl_2O_4$ master alloy.

After the formation of the first layer of $MgAl_2O_4$, Mg, Al, and Ti must diffuse through the layer to enable a further reaction at the interface of the TiO_2 particle. The reactive wetting continues until the particle surface is completely reacted. When $MgAl_2O_4$ crystals get accumulated and cover the entire TiO_2 particle surface, the reaction is likely to cease. Small $MgAl_2O_4$ crystals of a few hundred nm bonded by Van der Waals force remain clustered on the surface of a TiO_2 particle (event (b) in Figure 6). This mechanism is very similar to the formation and clustering of $MgAl_2O_4$ crystals on SiO_2 particles reported elsewhere.[21] In a parallel process, Ti atoms are released from TiO_2 and diffuse into molten Al. Fine Al_3Ti blocks (1 to 2 μm) clustered along with $MgAl_2O_4$ particles in partially dispersed agglomerates (Figures 2(c) and 5) testify for Al_3Ti formation during the reaction. The migration of Ti atoms across the TiO_2-Al interface initiates the overall diffusion process in the Al–Ti alloy system[25] but also can produce a saturated solution adjacent to the interface as a result of low solubility of Ti in Al [~0.8 wt pct at 1173 K (850 °C)], resulting in the nucleation of the Al_3Ti phase at the interface.[26] Fine Al_3Ti particles grow to larger ones either by interdiffusion of Al and Ti or by coalescence of fine Al_3Ti particles as shown by arrows in Figure 5. Thus, the complete reaction of TiO_2 with the Al-Mg melt is not possible without efficient dispersion of $MgAl_2O_4$ and Al_3Ti, enabling the progression of the reaction, and ultrasonic cavitation was found to facilitate the process.

3. *Effect of ultrasonication on dispersion of particles*

Ultrasonic processing was used as part of the procedure to synthesize the master alloy. The analysis of the master alloy showed that the TiO_2 particles reacted completely and that $MgAl_2O_4$ particles and fine agglomerates were dispersed within the matrix. The influence of

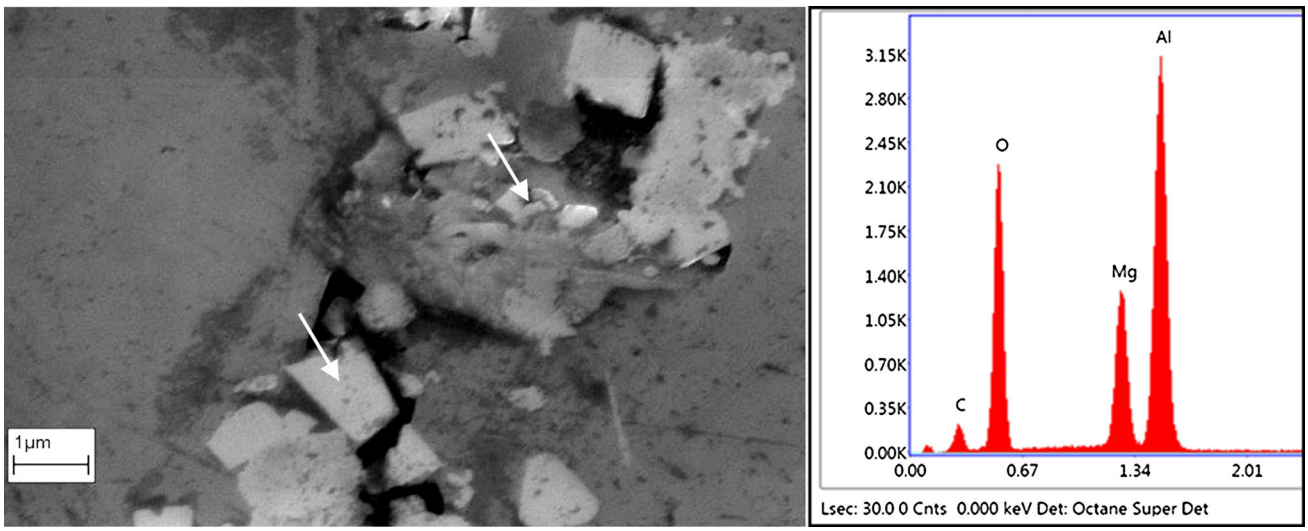

Fig. 4—SEM and EDS spectrum of $MgAl_2O_4$ dispersed in Al-Ti-$MgAl_2O_4$ master alloy.

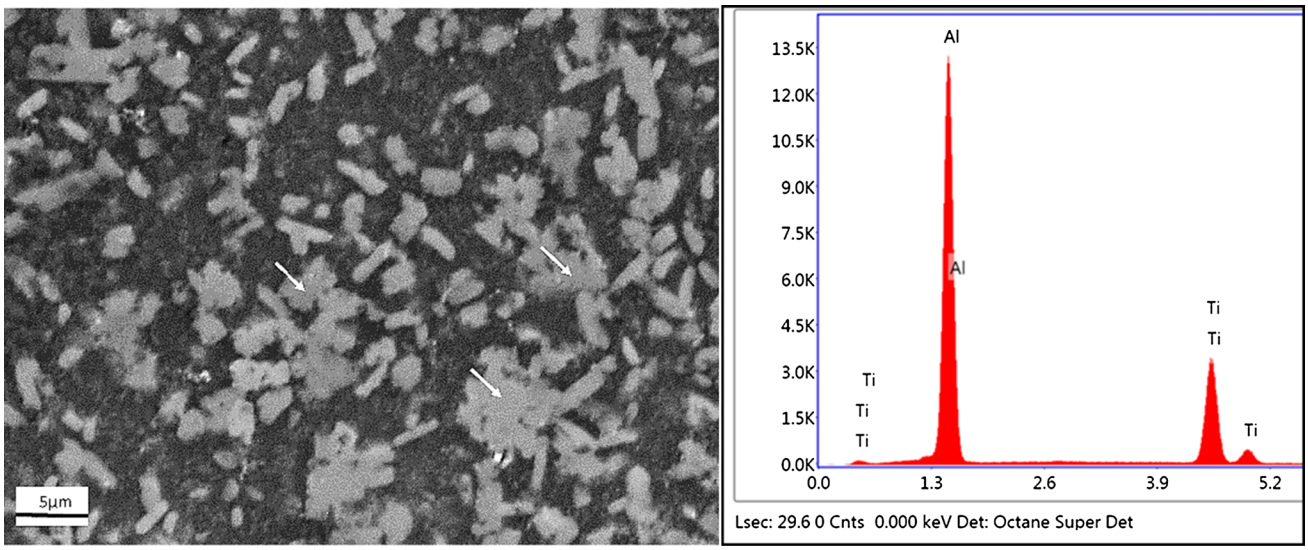

Fig. 5—SEM and EDS spectrum of Al_3Ti dispersed in Al-Ti-$MgAl_2O_4$ master alloy.

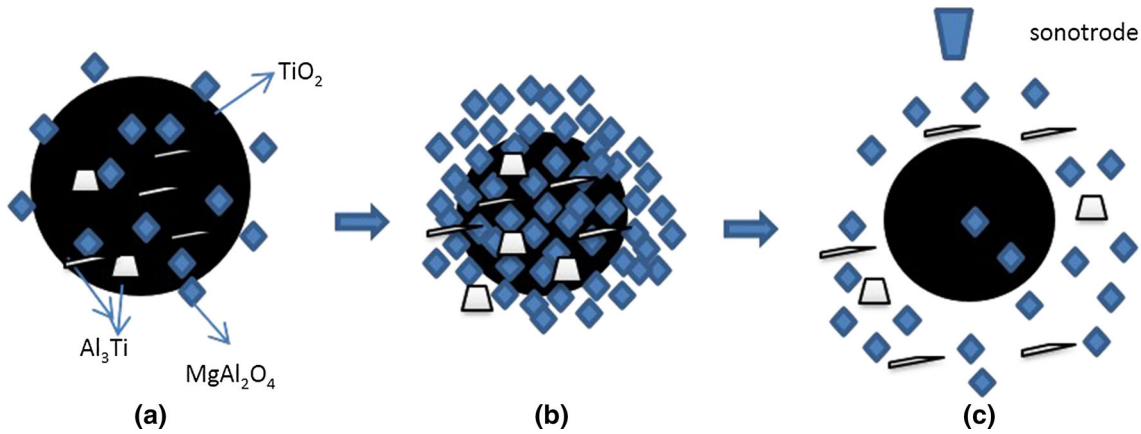

Fig. 6—Schematic of spinel dispersion in Al (*a*) reaction of oxides, (*b*) clustering of spinel and Al_3Ti, and (*c*) disintegration of clusters.

ultrasonic cavitation and acoustic streaming on the dispersion of ultrafine particles in molten metal has been studied elsewhere.[25,27–30] It was experimentally demonstrated that the cavitation threshold pressure reduced from 800 to 550 kPa with the increase in alumina concentration in an aluminum melt from 0.005 to 0.1 wt pct.[27] In the present experimental conditions, particles of TiO_2 and reaction products and gases absorbed on their surface act as nucleation sites for cavitation. Recently, Tzanakis *et al.*[31] reported that acoustic pressures exerted from the activity of the cavitation bubbles in liquid aluminum could be as high as 800 kPa, which may be sufficient to break the cluster of particles facilitating the de-agglomeration process and wetting. Cavitation and acoustic flows generated by the cavitation regions in a particle-populated molten metal may trigger the following events in the process under current investigation: (1) disintegration and distribution of loose TiO_2 agglomerates, (2) improved wetting and accelerated displacement reaction at particle interfaces, and (3) removal of $MgAl_2O_4$ clusters and the Al_3Ti phase from the reacted zone exposing a new diffusion zone for further reaction (event (c) in Figure 6). The mechanism is similar to the ultrasonic dispersion of *in situ* $MgAl_2O_4$[21] and *in situ* Al_3BC[32] crystals in Al-Mg-SiO_2 and Al-B-graphite alloys, respectively.

Particles of Al_3Ti are apparently refined during ultrasonic processing at 973 K to 993 K (700 °C to 720 °C). To confirm the cavitation-induced fragmentation of Al_3Ti, 100 g of master alloy was remelted at 1173 K (900 °C) and cast without ultrasonication. Large Al_3Ti needles over 200 μm in size were formed in the master alloy (Figure 7).

B. *Grain Refinement of an A357 Alloy*

1. *Effect of master alloy additions and ultrasonic melt processing on the grain size*

Figure 8 shows the microstructures of an anodized A357 alloy without additions. The average grain size of the unrefined alloy was 900 μm (Figure 8(a)). With the application of ultrasound but without master alloy

additions, the grain size of the alloy was found to be similar (Figure 8(b)). Upon the addition of 0.25 wt pct master alloy, the grain size was reduced to 640 μm (Figure 9 (a)). With further addition of master alloy from ~1.7 to 5.8 wt pct, grain size was reduced from 400 to 320 μm (Figures 9(b) and (c)). Application of ultrasonic processing gives further reduction of the grain size (~200 μm) at the higher addition levels of the master alloy; yet, the influence was less significant at the lowest addition (0.25 wt pct) (Figures 10(a) through (c)). The average grain size *vs* the amount of master alloy addition is shown in Figure 11. The plateau that represents the bottom limit of the grain size obtained with ultrasonication is about 200 μm and does not depend on the addition level from 1.7 wt pct onward. Figure 9 shows large pores and agglomerates in the microstructure of the grain refined alloys; nevertheless, defects are reduced appreciably after ultrasonic processing (Figure 10). This may be related to better distribution of spinel particles as a result of ultrasonic cavitation and induced flows as well as to the melt degassing by ultrasonic processing.[27]

To look at the significance of the new master alloy in grain refinement of A357 alloy, similar experiments were conducted with the addition of an Al-5Ti-1B master alloy. As the compositions of the two master alloys were different, the experiment with Al-5Ti-1B was conducted based on the similar free Ti content in the added master alloys. Free Ti content in the Al-Ti-$MgAl_2O_4$ and Al-5Ti-1B master alloys is ~1.3 and ~3 wt pct, respectively. The used additions of the master alloys and the corresponding free Ti concentrations are summarized in Table I.

The grain sizes of the A357 alloys with additions of either the commercial Al-5Ti-1B grain refiner or the spinel-based master alloy are compared on the basis of the free Ti in Figure 12. It is evident that at low addition levels, Al-5Ti-1B is more effective in grain size reduction than is the new oxide-containing master alloy. Nevertheless, at higher addition levels (equivalent to 0.02 wt pct of free Ti and beyond), both master alloys performed similarly. It is important to note that the amount of an Al-5Ti-1B master alloy required for achieving grain refinement is much lower than that of the oxide-containing master alloy in all the experiments (see Table I). Ultrasonication showed extra reduction in grain size at all additions. These observations are further confirmed from the microstructures of A357 alloys with different additions of the Al-5Ti-1B master alloy (Figures 13 and 14).

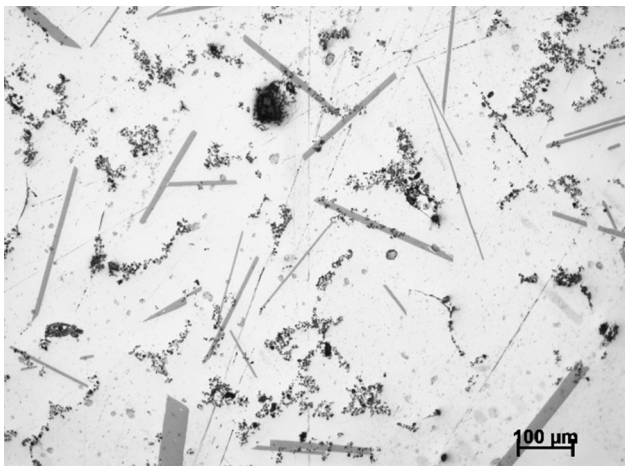

Fig. 7—Optical micrograph of remelted Al-Ti-$MgAl_2O_4$ master alloy.

2. *Mechanisms of grain refinement*

Thermal analysis is usually used to assess solidification of alloys, as are those inoculated with potential grain refiner inoculants. Figure 15 presents the representative cooling curves of an A357 alloy with and without 2 wt pct addition of the Al-Ti-$MgAl_2O_4$ master alloy, cast in the same metallic mold to measure the undercooling and the nucleation temperature of the primary Al grains. From these cooling curves, the nucleation temperature (T_n) of primary Al crystals is identified from the first derivative of the temperature (dT/dt) curve, where the slope of the T–t curve starts to deviate.[10] The other two characteristic temperatures are (1) T_{min}, unsteady state growth temperature or the onset of recalescence, when the latent heat of solidification surpasses the heat extracted from the sample by cooling; and (2) T_g, the end of recalescence or the onset of steady state growth of primary (Al) dendrites. Consequently,

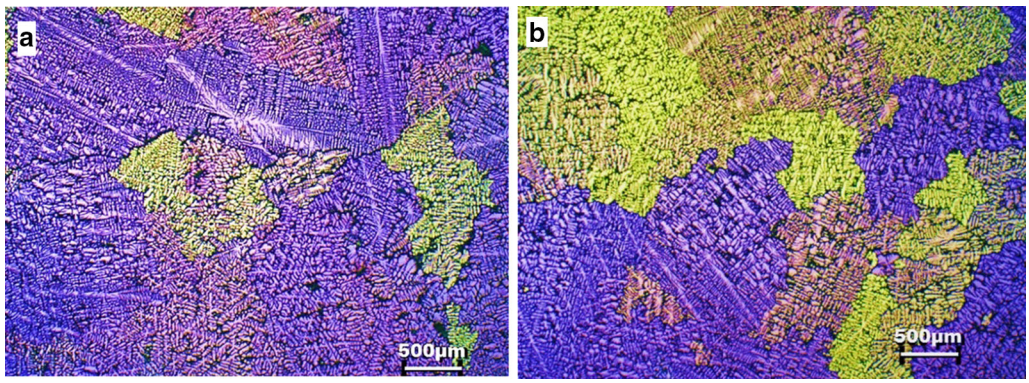

Fig. 8—Anodized micrographs of A357 cast (*a*) without ultrasonication and (*b*) with ultrasonication.

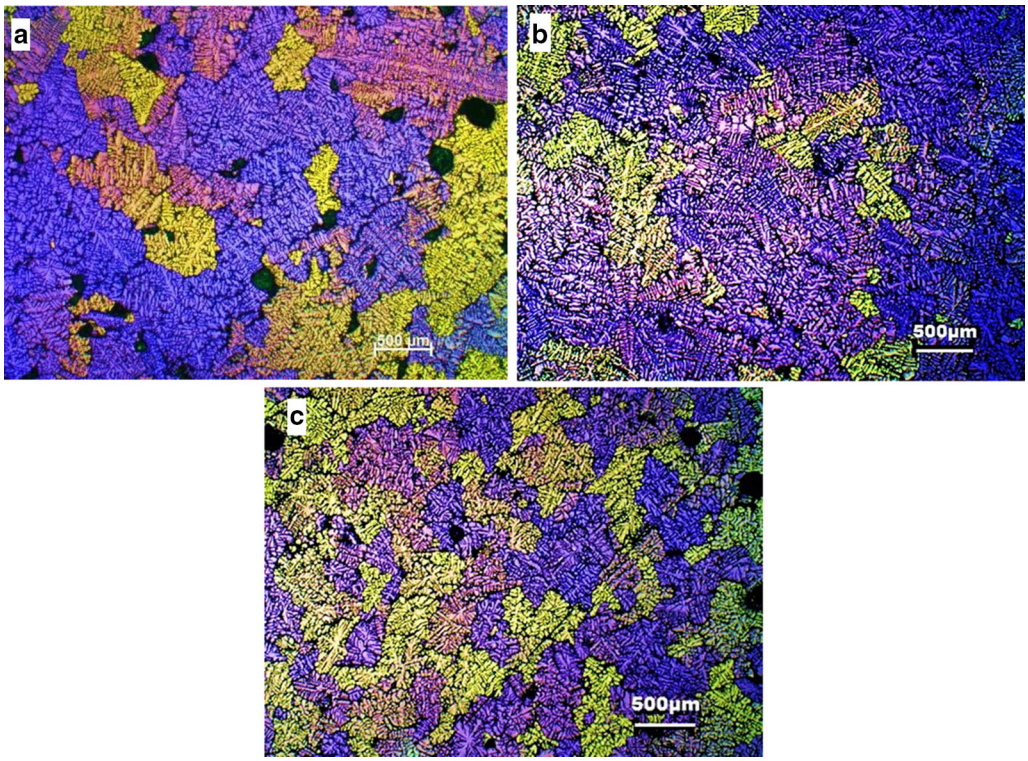

Fig. 9—Anodized micrographs of A357 cast without ultrasonication after inoculation of Al-Ti-$MgAl_2O_4$ (*a*) 0.25 wt pct, (*b*) 1.7 wt pct, and (*c*) 5.8 wt pct.

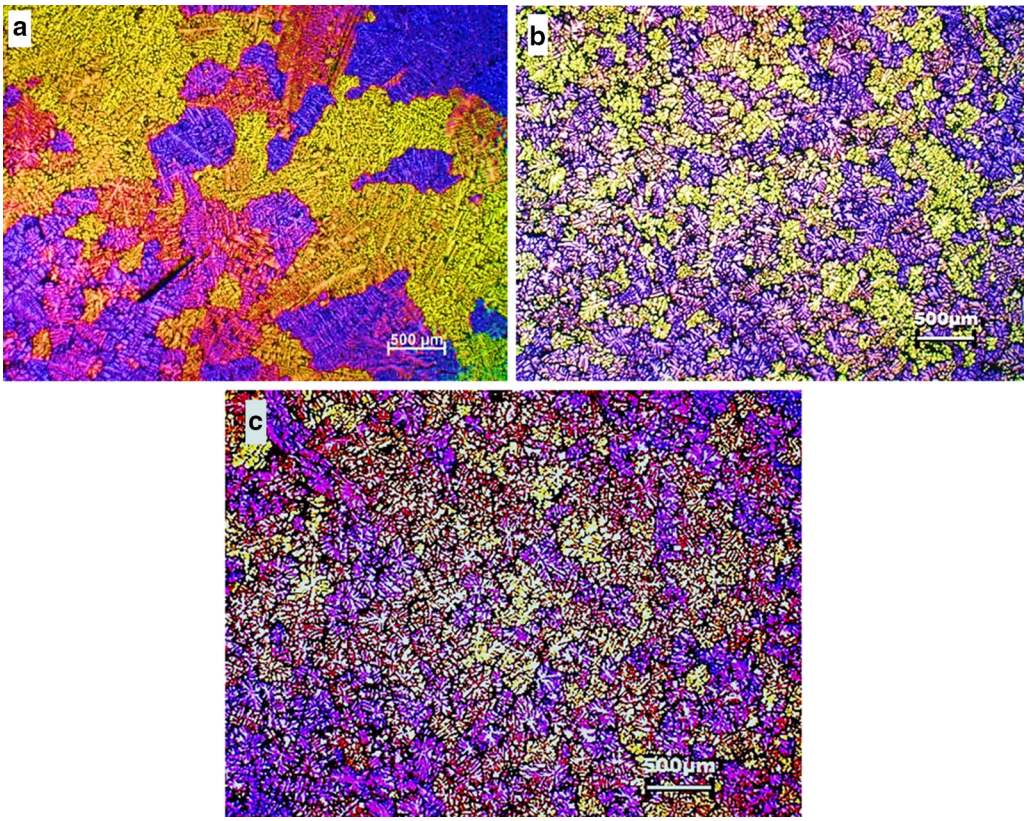

Fig. 10—Anodized micrographs of A357 cast with ultrasonication after inoculation of Al-Ti-$MgAl_2O_4$ (*a*) 0.25 wt pct, (*b*) 1.7 wt pct, and (*c*) 5.8 wt pct.

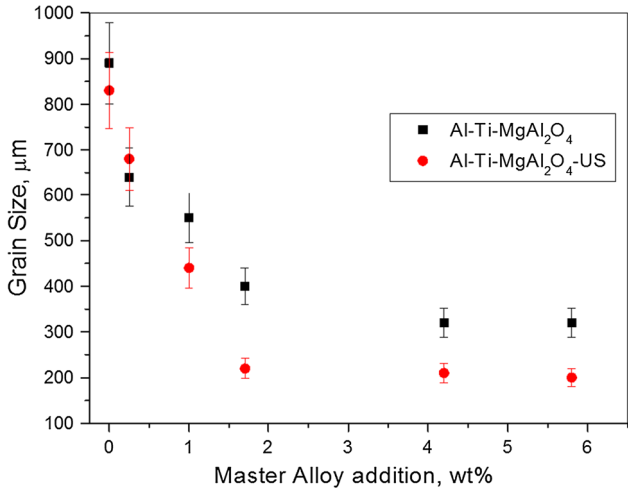

Fig. 11—Relation between grain size of A357 and the level of Al-Ti-$MgAl_2O_4$ master alloy addition.

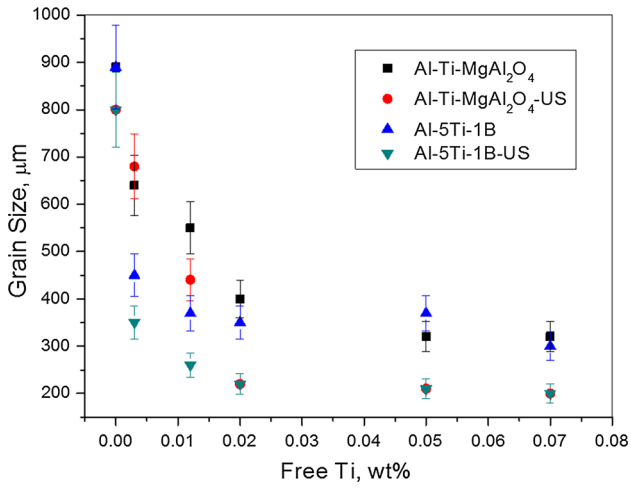

Fig. 12—Relation between grain size of A357 and the free Ti from the added master alloys.

Table I. Master Alloy Additions and Corresponding Free Ti in Each Master Alloy, Respectively (in Wt Pct)

Master Alloy	Addition (Wt Pct)	Free Ti (Wt Pct)
Al-Ti-$MgAl_2O_4$	0.25, 1.0, 1.7, 4.2, 5.8	0.003, 0.012, 0.02,
Al-5Ti-1B	0.1, 0.4, 0.7, 1.7, 2.4	0.05, 0.07

the undercooling of the primary (Al) nucleation can be approximated as $\Delta T = (T_g - T_{min})$.[10] In the alloy without master alloys addition (Figure 15 (a)), the (Al) primary phase starts to nucleate at 893 K (620 °C) and ends at 891.5 K (618.5 °C). The maximum nucleation undercooling from the recalescence was calculated to be 1.5 K (1.5 °C). In the presence of the Al-Ti-$MgAl_2O_4$ master alloy (Figure 15(b)), (Al) in the A357 alloy starts nucleating at a higher temperature of ~896 K (623 °C) (up nearly by 3 K (3 °C)) and no nucleation undercooling was noticed in the cooling curve. It was reported earlier that the Ti presence in an inoculated A356 alloy increased its liquidus temperature and, hence, the nucleation started higher in the cooling curve.[33] The absence of recalescence is not uncommon in Al-Si alloys inoculated with a higher amount of Al-5Ti-1B master alloy and at moderate cooling rates, *e.g.*, 2 K/s (2 °C/s).[34,35] This happens as a result of an increased number of heterogeneous nucleation events aided by numerous nucleant particles present in the alloy at higher additions of master alloy (2 wt pct here). Note that the limitations of the data acquisition and thermocouple sensitivity can sometimes neglect a small change in the temperature. The results of this thermal analysis testify that $MgAl_2O_4$ particles act as potent heterogeneous nucleation sites for aluminum.

The nucleation potency of a substrate is related to its lattice matching with solid Al during nucleation process. A closer lattice match refers to better nucleation potency. Lattice matching of $MgAl_2O_4$ with Al was experimentally reported to be a cube on a cube parallel orientation relationship (OR),[36] or a mismatch of 2.5 deg along the [110] direction on the (111) plane between Al and $MgAl_2O_4$[37] with a theoretically calculated misfit of 1.4 pct.[13] This mismatch was found to be smaller than that of the Al/TiB_2 system (−4.2 pct).[13] The nucleation efficiency has also direct correlation with the number density and size distribution of particles and the undercooling (cooling conditions). According to the athermal heterogeneous nucleation theory, the nucleation undercooling, ΔT_g, can be estimated by the equation:[38]

$$\Delta T_g = 4\Gamma_{sl}/D \qquad [2]$$

where Γ_{sl} is the Gibbs–Thomson coefficient between the stable embryo of the solid phase and the liquid and D is the diameter of the particle. For an Al alloy, Γ_{sl} is about 9.12×10^{-8} K m.[38] From Eq. [2], the undercooling required for $MgAl_2O_4$ crystals to nucleate aluminum can be calculated as 1.82 K (1.82 °C) for 200-nm particles and 0.18 K (0.18 °C) for 2-μm particles. It was also shown that for four contributions to the total solidification undercooling (kinetic, curvature, thermal, and solutal), the solutal or constitutional undercooling (ΔT_{cs}) is the controlling term under typical aluminum alloy casting conditions.[39] Maximum ΔT_{cs} for CP Al at a typical solidification velocity was calculated to be 2.8 K (2.8 °C) and assumed to be higher for more solute-containing alloys.[40] The measured thermal undercooling is very small in the case of spinel-inoculated alloys (Figure 15). This means that the solutal component of undercooling plays the most essential role in nucleation on the $MgAl_2O_4$ substrates.

It is well known that with a spread of particle sizes, grain initiation events are also spread over a range of undercooling.[39,40] A few early nucleation events triggered by larger particles can then lead to grain growth and latent heat evolution, rendering many smaller particles inactive. In was shown that in the Al-5Ti-1B master alloy, active TiB_2 particles constitute around 40 vol pct of the particles population but the number

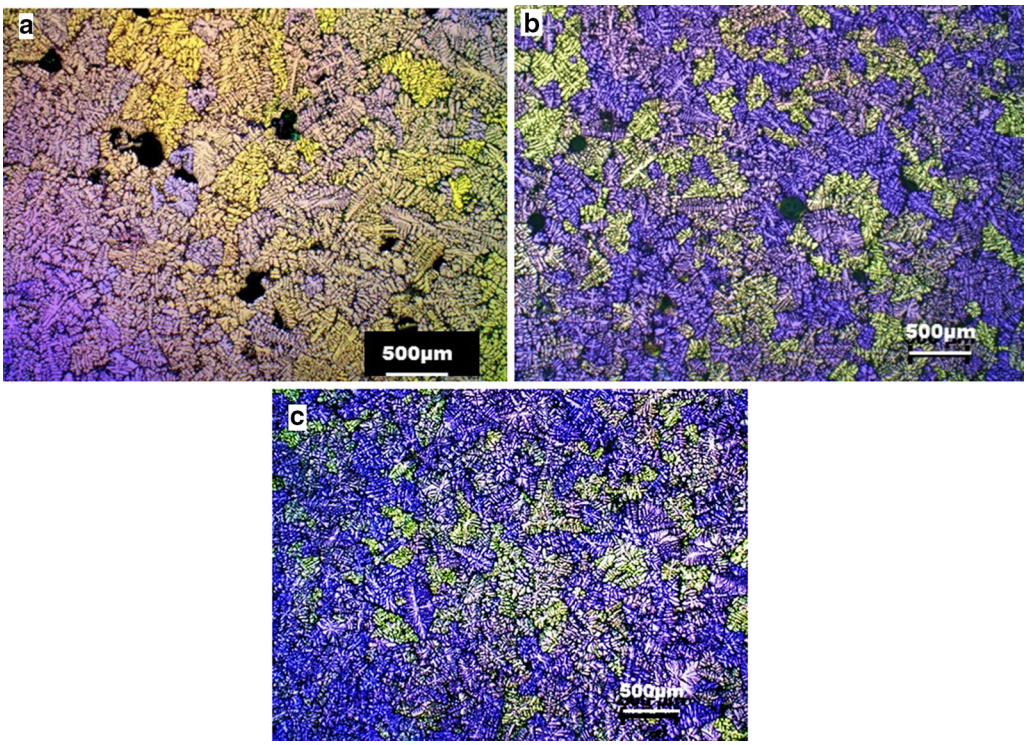

Fig. 13—Anodized micrographs of A357 cast without ultrasonication after inoculation of Al-5Ti-1B (*a*) 0.003 wt pct, (*b*) 0.02 wt pct, and (*c*) 0.07 wt pct free Ti.

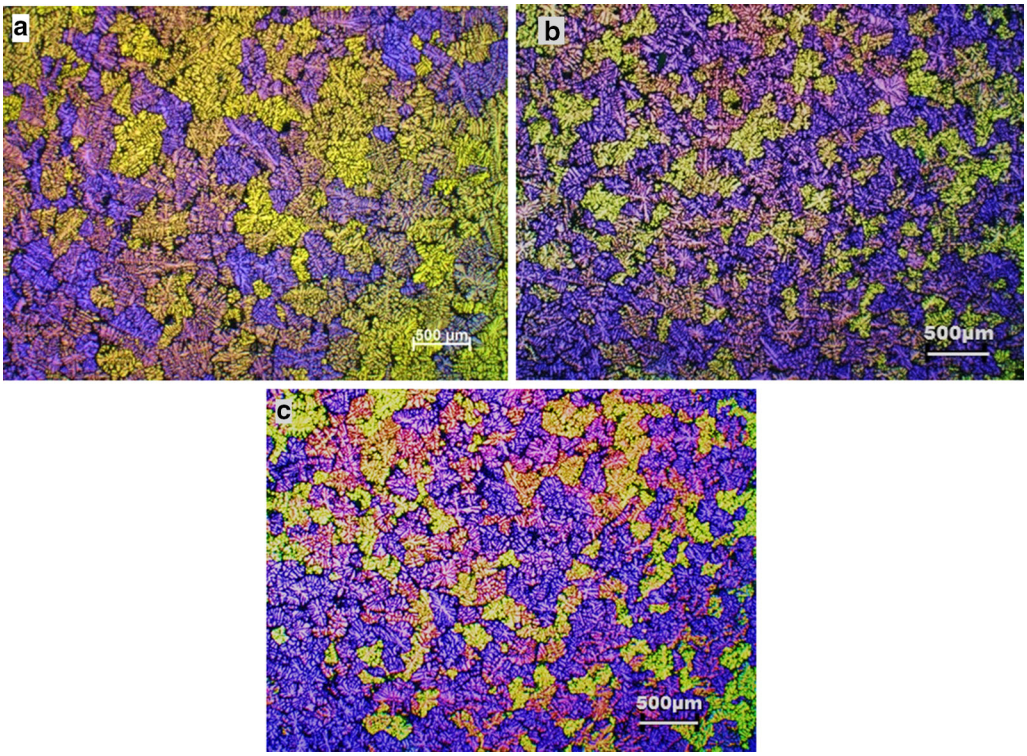

Fig. 14—Anodized micrographs of A357 cast with ultrasonication after inoculation of Al-5Ti-1B (*a*) 0.003 wt pct, (*b*) 0.02 wt pct, and (*c*) 0.07 wt pct free Ti.

efficiency of optimum sized particles is less than 1 pct.[40] Furthermore, particles less than 500 nm in size do not take part in nucleation even under cooling rates as high as ~3.5 K/s (3.5 °C/s). At lower cooling rates, as in the study, ~2 to 3 K/s (2 to 3 °C/s), the minimum particle size will be much larger. Hence, the best nucleation

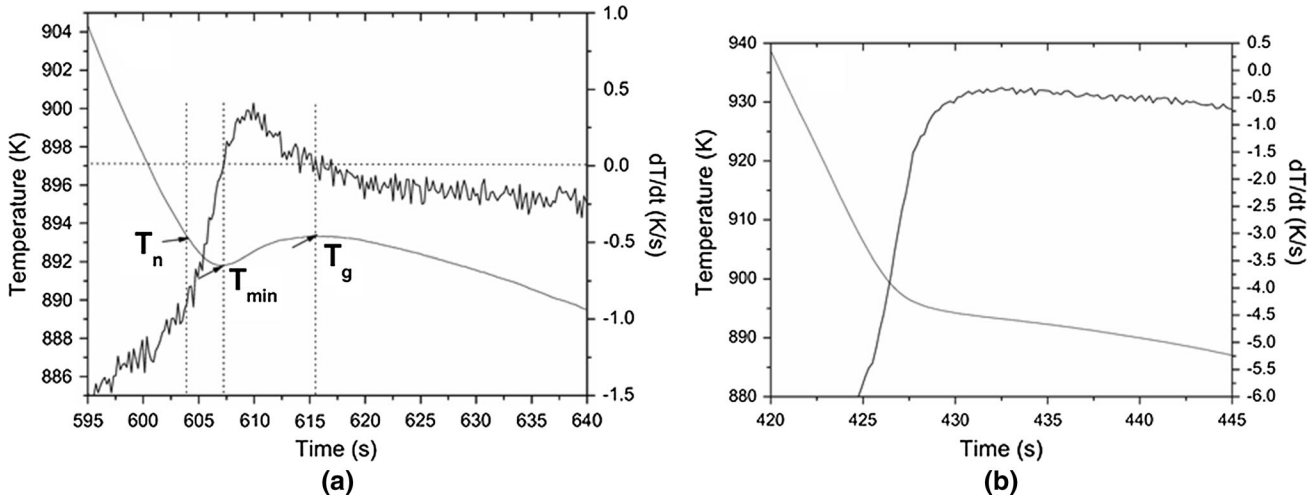

Fig. 15—Cooling curves of (*a*) A357 and (*b*) A357 inoculated with 2 wt pct Al-Ti-$MgAl_2O_4$ master alloy.

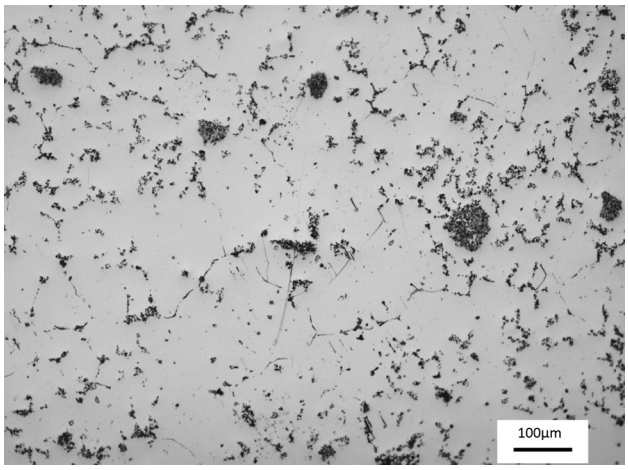

Fig. 16—Optical micrographs of Al-Si-$MgAl_2O_4$ master alloy.

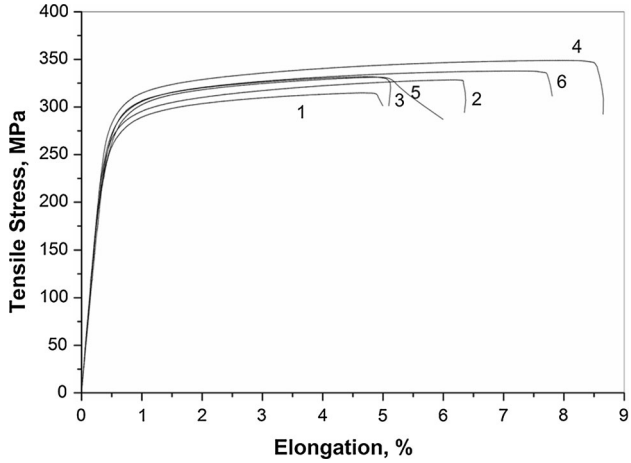

Fig. 18—Stress–strain curves for tensile testing of different A357 alloys inoculated with Al-Ti-$MgAl_2O_4$ and Al-5Ti-1B master alloys and treated with ultrasound (Details in Table II).

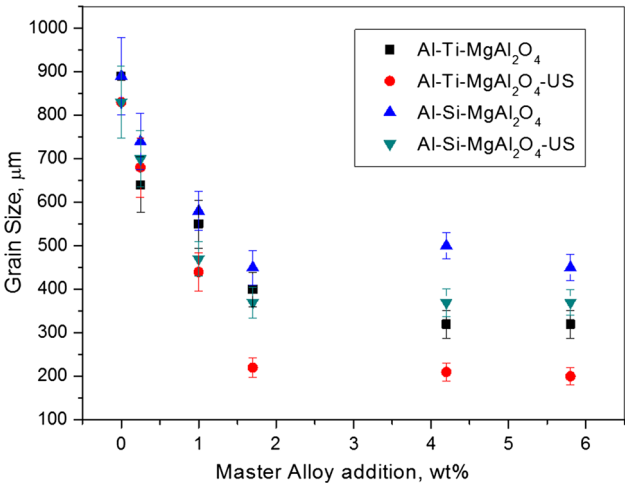

Fig. 17—Comparison of grain size with the addition of Al-Ti-$MgAl_2O_4$ (this study) and Al-Si-$MgAl_2O_4$[14] master alloys in A357.

efficiency under real casting conditions is achieved by decreasing the spread of particle distribution and increasing the particle size ideally to 2 to 5 μm.[40] Our results show that $MgAl_2O_4$ particles in the Al-Ti-$MgAl_2O_4$ master alloy have a large spread of particles sizes, from a few hundred nm to 2 microns. For a particular free Ti level, the number density of $MgAl_2O_4$ particles in the Al-Ti-$MgAl_2O_4$ master alloy is higher than that of TiB_2 in Al-5Ti-1B. Nevertheless, the spinel-containing master alloy may largely contain very small particles (*i.e.*, inactive particles), which negatively affects the nucleation efficiency of this master alloy. This is evident at lower additions of the master alloy where grain size was found to be larger than those produced with an optimized commercial Al-5Ti-1B grain refiner. More addition seemingly increased the number density required for the grain refinement to the level similar to Al-5Ti-1B. Yet, a large number of inactive particles in the Al-Ti-$MgAl_2O_4$ master alloy did not contribute to

Table II. Mechanical Properties of A357 Alloy Inoculated with Different Master Alloys and Treated With Ultrasonication

No	Alloy	Yield Stress (MPa)	Ultimate Tensile Stress (MPa)	Elongation (Pct)
1	A357	260 ± 8	314 ± 8	5 ± 1
2	A357-US	273 ± 5	326 ± 6	6 ± 1
3	A357-MA	278 ± 3	337 ± 9	5 ± 2
4	A357-MA-US	288 ± 4	349 ± 9	8 ± 2
5	A357-Al5Ti1B	272 ± 5	335 ± 10	5 ± 2
6	A357-Al5Ti1B-US	278 ± 7	340 ± 9	7 ± 2

grain refinement even if they were well distributed, which required larger addition level.

The influence of ultrasonication on the grain refinement of alloys treated above the liquidus was studied extensively.[27] A systematic study by Wang *et al.*[41] in a noninoculated alloy made clear that ultrasonication in a complete liquid state had a negligible effect on grain refinement, which was substantiated in the present study. Nevertheless, the additional grain refinement was observed when ultrasonication was applied to the liquid metal containing $MgAl_2O_4$ or TiB_2 particles. Additional grain size reduction by ultrasonication suggests that this treatment helped in distributing the active particles of TiB_2 or $MgAl_2O_4$ in the liquid metal. Recent work showed that ultrasonication was capable of dispersion of *in situ* $MgAl_2O_4$ particulates in liquid metal, while manual or mechanical stirring apparently failed to distribute fine particles in the liquid metal.[14,21]

The presence of free Ti in the master alloy adds to the grain-refining effect through growth restriction. This becomes evident if one compares the results reported on the grain refinement by a similar master alloy with spinel but without Ti[14] (Figure 16) with the results reported in this article. For the reader's convenience, the data are summarized in Figure 17. Although the alloy contains ~0.1 wt pct of Ti, formation of the Al-Ti-Si phase[42] diminishes the free Ti available for growth restriction. As a result, large grains (900 μm) and long dendrite arms are formed during solidification. With the addition of Al-Si-$MgAl_2O_4$ master alloy, the grain size is reduced to 450 to 350 μm, implying the heterogeneous nucleation by $MgAl_2O_4$. Further reduction of 100 to 150 μm with the addition of Al-Ti-$MgAl_2O_4$ master alloy suggests a possible growth restriction by the extra Ti (0.02-0.06 wt pct) in the form of Al_3Ti from the master alloy. A similar mechanism is explained for A356 alloy inoculated with Al-5Ti-1B master alloy.[43]

C. *Mechanical Properties of A357 Alloys*

Mechanical behavior of A357 alloys cast under different conditions, with and without grain refiner, is shown in Figure 18 and Table II.

A systematic improvement in both strength and ductility with respect to the addition of the oxide-containing master alloy and ultrasonication is obvious. A minimum of 10 and 50 pct increase in strength and ductility, respectively, was achieved in an A357 alloy inoculated with oxides and treated with ultrasonic cavitation in comparison with the reference alloy. Moreover, the strength and ductility of the oxide inoculated alloys are comparable with the alloys inoculated with an equivalent amount of Al-5Ti-1B master alloy (0.02 wt pct free Ti). In addition to the grain refinement of the inoculated alloys, the ultrasonic cavitation and streaming additionally contribute to the improvement of mechanical properties by reducing hydrogen porosity but redistribution of nonmetallic inclusions.[27]

IV. CONCLUSIONS

1. An Al-1.3 wt pct Ti-1.8 wt pct $MgAl_2O_4$ master alloy was successfully manufactured using an ultrasonication-aided *in situ* synthesis. Complete reaction of the parent TiO_2 oxide with a homogeneous bulk distribution of formed $MgAl_2O_4$ particles and their clusters was achieved by this methodology. Fine particles of Al_3Ti (2 to 20 μm) were also formed and distributed in the alloy.
2. The master alloy is capable of grain refining an A357 alloy (Al-7 pct Si-0.5 pct Mg) by 50 pct. Ultrasonication is responsible for further grain refinement by 25 pct. Spinel particles in the master alloy provide substrates for aluminum nucleation, whereas free Ti restricts grain growth.
3. The master alloy showed similar grain refinement performance in comparison with a commercial Al-5Ti-1B master alloy if compared on the free added Ti level, albeit at a higher master alloy addition.
4. Grain refinement with oxide inoculation and ultrasonic processing of an A357 alloy resulted in at least 10 pct strength and 50 pct elongation improvement in comparison with the reference alloy and a similar mechanical performance in comparison with the alloys inoculated with Al-5Ti-1B master alloy.

ACKNOWLEDGMENT

The authors wish to acknowledge financial support from the ExoMet Project, which is co-funded by the European Commission in the 7th Framework Program (Contract FP7-NMP3-LA-2012-280421), by the European Space Agency, and by the individual partner organizations.

REFERENCES

1. D.G. McCartney: *Int. Mater. Rev.*, 1989, vol. 34, pp. 247–60.
2. B.S. Murty, S.A. Kori, and M. Chakraborty: *Int. Mater. Rev.*, 2002, vol. 47, pp. 3–29.
3. K.T. Kashyap and T. Chandrasekhar: *Bull. Mater. Sci.*, 2001, vol. 24, pp. 345–53.
4. M. Easton and D.H. St John: *Metall. Mater. Trans.*, 1999, vol. 30A, pp. 1613–23.
5. P.S. Mohanty and J.E. Gruzleski: *Acta Metall. Mater.*, 1995, vol. 43, pp. 2001–12.
6. P. Schumacher and A.L. Greer: *Mater. Sci. Eng. A*, 1994, vol. 178, pp. 309–13.
7. F. Wang, Z. Liu, D. Qiu, J.A. Taylor, M.A. Easton, and M.X. Zhang: *Acta Mater.*, 2013, vol. 61, pp. 360–70.
8. Y. Birol: *J. Alloys Comp.*, 2007, vol. 440, pp. 108–12.
9. V.H. Lopez, A. Scoles, and A.R. Kennedy: *Mater. Sci. Eng. A*, 2003, vol. 356, pp. 316–25.
10. M. Nowak, L. Bolzoni, and N. Hari Babu: *Mater. Des.*, 2015, vol. 66, pp. 366–75.
11. A.L. Greer: *Philos. Trans. R. Soc. Lond. A*, 2003, vol. 361, pp. 479–95.
12. M.A. Easton, M. Qian, A. Prasad, and D.H. St John: *Curr. Opin. Solid State Mater. Sci.*, 2016, vol. 20 (1), pp. 13–24.
13. H.T. Li, Y. Wang, and Z. Fan: *Acta Mater.*, 2012, vol. 60, pp. 1528–37.
14. V.M. Sreekumar, N.H. Babu, D.G. Eskin, and Z. Fan: *Mater. Sci. Forum*, 2014, vol. 155, pp. 794–96.
15. K. Kim: *Metall. Mater. Trans. A*, 2014, vol. 45 (10), pp. 4538–48.
16. Y. Kim and J.C. Lee: *Mater. Sci. Eng A*, 2006, vol. 420, pp. 8–12.
17. M. Hanabe and P.B. Aswath: *Acta Mater.*, 1997, vol. 45, pp. 4067–76.
18. D. Horvitz and I. Gotman: *Acta Mater.*, 2002, vol. 50, pp. 1961–71.
19. Z. Yu, N. Zhao, E. Liu, C. Shi, X. Du, and J. Wang: *Composites: Part A*, 2012, vol. 43, pp. 631–34.
20. T.V. Atamanenko, D.G. Eskin, L. Zhang, and L. Katgerman: *Metall. Mater. Trans. A*, 2010, vol. 41, pp. 2056–66.
21. V.M. Sreekumar, N.H. Babu, D.G. Eskin, and Z. Fan: *Mater. Sci. Eng. A*, 2015, vol. 628, pp. 30–40.
22. P.C. Maity, S.C. Panigrahi, and P.N. Chakraborty: *Scripta Metall. Mater.*, 1993, vol. 28, pp. 549–52.
23. V.M. Sreekumar, K.R. Ravi, R.M. Pillai, B.C. Pai, and M. Chakraborty: *Metall. Mater. Trans. A*, 2008, vol. 39, pp. 919–33.
24. V.M. Sreekumar: Ph.D. Dissertation, 2008, Indian Institute of Technology, Kharagpur.
25. Z. Liu, Q. Han, and J. Li: *Powder Technol.*, 2013, vol. 247, pp. 55–59.
26. M. Yan and Z. Fan: *J. Mater. Sci.*, 2001, vol. 36, pp. 285–95.
27. G.I. Eskin and D.G. Eskin: *Ultrasonic Treatment of Light Alloy Melts*, 2nd ed., CRC Press, Boca Raton, FL, 2014.
28. O.V. Abramov: *Ultrasound in Liquid and Solid Metals*, CRC Press, Boca Raton, FL, 1994, pp. 43–77, 273–406.
29. K.S. Suslick and G.J. Price: *Annu. Rev. Mater. Sci.*, 1999, vol. 29, pp. 295–326.
30. J. Yan, Z. Xu, L. Shi, X. Ma, and S. Yang: *Mater Des.*, 2011, vol. 32, pp. 343–47.
31. I. Tzanakis, G.S.B. Lebon, D.G. Eskin, and K.A. Pericleous: *J. Mater. Process. Tech.*, 2016, vol. 229, pp. 582–86.
32. U. Joshi, V.M. Sreekumar, N. HariBabu, and D.G. Eskin: *Metall. Mater. Trans. A*, 2015, vol. 46, pp. 2862–69.
33. S. Nafisi and R. Ghomashchi: *J. Mater. Proc. Tech.*, 2006, vol. 174, pp. 371–83.
34. S.M. Jigajinni, K. Venkateswarlu, and S.A. Kori: *Int. J. Eng. Sci. Tech.*, 2011, vol. 3 (6), pp. 257–72.
35. V. Gutiérrez, G. González, and A. García: *Chem. Mater. Res.*, 2014, vol. 6 (6), pp. 52–62.
36. R. Schweinfest, S. Köstlmeier, F. Ernst, C. Elsäser, T. Wagner, and M.W. Finnis: *Philos. Magn.*, 2001, vol. 81 (4), pp. 927–55.
37. Z.P. Luo: *Acta Mater.*, 2006, vol. 54, pp. 47–58.
38. J.A. Dantzig and M. Rappaz: *Solidification*, CRC Press, Boca Raton, FL, 2009.
39. T.E. Quested and A.L. Greer: *Acta Mater.*, 2004, vol. 52, pp. 3859–68.
40. T.E. Quested and A.L. Greer: *Acta Mater.*, 2005, vol. 53, pp. 4643–53.
41. G. Wang, M.S. Dargusch, M. Qian, D.G. Eskin, and D.H. St: John*J. Cryst. Growth.*, 2014, vol. 8, pp. 119–24.
42. X.G. Chen and M. Fortier: *J. Mater. Proc. Tech.*, 2010, vol. 210 (13), pp. 1780–86.
43. S. Nafisi and R. Ghomashchi: *J. Mater. Proc. Tech.*, 2006, vol. 174, pp. 371–83.